NATURE | **ARTICLE**

日本語要約

Stimulus-triggered fate conversion of somatic cells into pluripotency

Haruko Obokata, Teruhiko Wakayama, Yoshiki Sasai, Koji Kojima, Martin P. Vacanti, Hitoshi Niwa, Masayuki Yamato & Charles A. Vacanti

Nature **505**, 641–647 (30 January 2014) doi:10.1038/nature12968
Received 10 March 2013 Accepted 20 December 2013 Published online 29 January 2014

Abstract

Here we report a unique cellular reprogramming phenomenon, called stimulus-triggered acquisition of pluripotency (STAP), which requires neither nuclear transfer nor the introduction of transcription factors. In STAP, strong external stimuli such as a transient low-pH stressor reprogrammed mammalian somatic cells, resulting in the generation of pluripotent cells. Through real-time imaging of STAP cells derived from purified lymphocytes, as well as gene rearrangement analysis, we found that committed somatic cells give rise to STAP cells by reprogramming rather than selection. STAP cells showed a substantial decrease in DNA methylation in the regulatory regions of pluripotency marker genes. Blastocyst injection showed that STAP cells efficiently contribute to chimaeric embryos and to offspring via germline transmission. We also demonstrate the derivation of robustly expandable pluripotent cell lines from STAP cells. Thus, our findings indicate that epigenetic fate determination of mammalian cells can be markedly converted in a context-dependent manner by strong environmental cues.

Subject terms: Reprogramming

Introduction

In the canalization view of Waddington's epigenetic landscape, fates of somatic cells are progressively determined as cellular differentiation proceeds, like going downhill. It is generally believed that reversal of differentiated status requires artificial physical or genetic manipulation of nuclear function such as nuclear transfer[1, 2] or the introduction of multiple transcription factors[3]. Here we investigated the question of whether somatic cells can undergo nuclear reprogramming simply in response to external triggers without direct nuclear manipulation. This type of situation is known to occur in plants—drastic environmental changes can convert mature somatic cells (for example, dissociated carrot cells) into immature blastema cells, from which a whole plant structure, including stalks and roots, develops in the presence of auxins[4]. A challenging question is whether animal somatic cells have a similar potential that emerges under special conditions. Over the past decade, the presence of pluripotent cells (or closely relevant cell types) in adult tissues has been a matter of debate, for which conflicting

conclusions have been reported by various groups[5, 6, 7, 8, 9, 10, 11]. However, no study so far has proven that such pluripotent cells can arise from differentiated somatic cells.

Haematopoietic cells positive for CD45 (leukocyte common antigen) are typical lineage-committed somatic cells that never express pluripotency-related markers such as Oct4 unless they are reprogrammed[12, 13]. We therefore addressed the question of whether splenic CD45$^+$ cells could acquire pluripotency by drastic changes in their external environment such as those caused by simple chemical perturbations.

Low pH triggers fate conversion in somatic cells

CD45$^+$ cells were sorted by fluorescence-activated cell sorting (FACS) from the lymphocyte fraction of postnatal spleens (1-week old) of C57BL/6 mice carrying an *Oct4-gfp* transgene[14], and were exposed to various types of strong, transient, physical and chemical stimuli (described below). We examined these cells for activation of the *Oct4* promoter after culture for several days in suspension using DMEM/F12 medium supplemented with leukaemia inhibitory factor (LIF) and B27 (hereafter called LIF+B27 medium). Among the various perturbations, we were particularly interested in low-pH perturbations for two reasons. First, as shown below, low-pH treatment turned out to be most effective for the induction of *Oct4*. Second, classical experimental embryology has shown that a transient low-pH treatment under 'sublethal' conditions can alter the differentiation status of tissues. Spontaneous neural conversion from salamander animal caps by soaking the tissues in citrate-based acidic medium below pH 6.0 has been demonstrated previously[15, 16, 17].

Without exposure to the stimuli, none of the cells sorted with CD45 expressed *Oct4*-GFP regardless of the culture period in LIF+B27 medium. In contrast, a 30-min treatment with low-pH medium (25-min incubation followed by 5-min centrifugation; Fig. 1a; the most effective range was pH 5.4–5.8; Extended Data Fig. 1a) caused the emergence of substantial numbers of spherical clusters that expressed *Oct4*-GFP in day-7 culture (Fig. 1b). Substantial numbers of GFP$^+$ cells appeared in all cases performed with neonatal splenic cells (n = 30 experiments). The emergence of *Oct4*-GFP$^+$ cells at the expense of CD45$^+$ cells was also observed by flow cytometry (Fig. 1c, top, and Extended Data Fig. 1b, c). We next fractionated CD45$^+$ cells into populations positive and negative for CD90 (T cells), CD19 (B cells) and CD34 (haematopoietic progenitors[18]), and subjected them to low-pH treatment. Cells of these fractions, including T and B cells, generated *Oct4*-GFP$^+$ cells at an efficacy comparable to unfractionated CD45$^+$ cells (25–50% of surviving cells on day 7), except for CD34$^+$ haematopoietic progenitors[19], which rarely produced *Oct4*-GFP$^+$ cells (<2%; Extended Data Fig. 1d).

Figure 1: Stimulus-triggered conversion of lymphocytes into *Oct4*-GFP$^+$ cells.

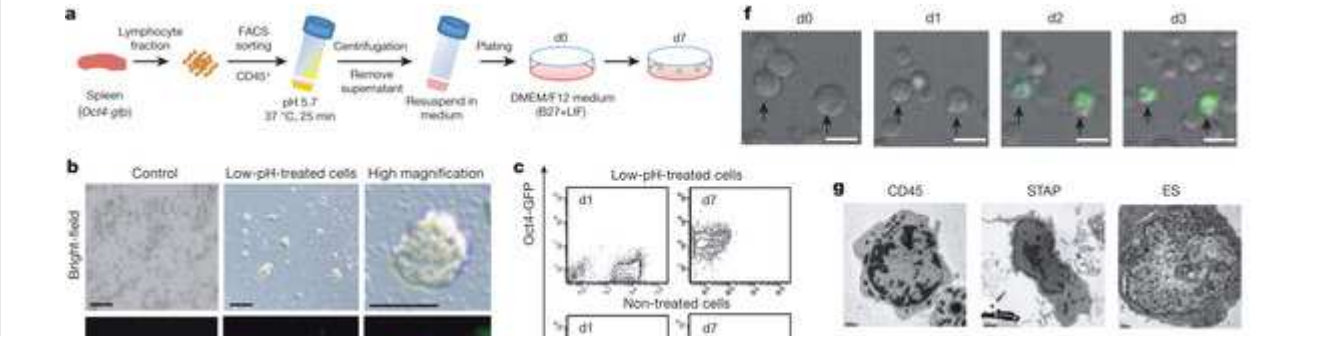

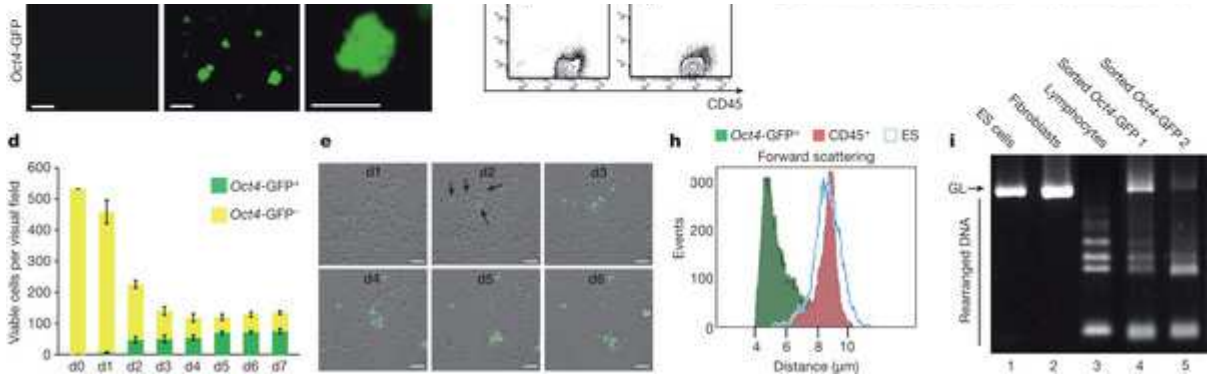

a, Schematic of low-pH treatment. **b**, *Oct4*-GFP$^+$ cell clusters appeared in culture of low-pH-treated CD45$^+$ cells (middle; high magnification, right) on day 7 (d7) but not in culture of control CD45$^+$ cells (left). Top: bright-field view; bottom, GFP signals. Scale bar, 100 μm. **c**, FACS analysis. The *x* axis shows CD45 epifluorescence level; *y* axis shows *Oct4*-GFP level. Non-treated, cultured in the same medium but not treated with low pH. **d**, GFP$^+$ (green) and GFP$^-$ (yellow) cell populations (average cell numbers per visual field; ×10 objective lens). *n* = 25; error bars show average ± s.d. **e**, Snapshots of live imaging of culture of low-pH-treated CD45$^+$ cells (*Oct4-gfp*). Arrows indicate cells that started expressing *Oct4*-GFP. Scale bar, 50 μm. **f**, Cell size reduction in low-pH-treated CD45$^+$ cells on day 1 before turning on *Oct4*-GFP without cell division on day 2. In this live imaging, cells were plated at a half density for easier viewing of individual cells. Scale bar, 10 μm. **g**, Electron microscope analysis. Scale bar, 1 μm. **h**, Forward scattering analysis of *Oct4*-GFP$^-$CD45$^+$ cells (red) and *Oct4*-GFP$^+$CD45$^-$ cells (green) on day 7. Blue line, ES cells. **i**, Genomic PCR analysis of (D)J recombination at the *Tcrb* gene. GL is the size of the non-rearranged germline type, whereas the smaller ladders correspond to the alternative rearrangements of J exons. Negative controls, lanes 1, 2; positive controls, lane 3; FACS-sorted *Oct4*-GFP$^+$ cells (two independent preparations on day 7), lanes 4, 5.

Among maintenance media for pluripotent cells[20], the appearance of *Oct4*-GFP$^+$ cells was most efficient in LIF+B27 medium, and did not occur in mouse epiblast-derived stem-cell (EpiSC) medium[21, 22] (Extended Data Fig. 1e). The presence or absence of LIF during days 0–2 did not substantially affect the frequency of *Oct4*-GFP$^+$ cell generation on day 7 (Extended Data Fig. 1f), whereas the addition of LIF during days 4–7 was not sufficient, indicating that LIF dependency started during days 2–4.

Most of the surviving cells on day 1 were still CD45$^+$ and *Oct4*-GFP$^-$. On day 3, the total cell numbers were reduced to between one-third to one-half of the day 0 population (Fig. 1d; see Extended Data Fig. 1g, h for apoptosis analysis), and a substantial number of total surviving cells became *Oct4*-GFP$^+$ (Fig. 1d), albeit with relatively weak signal intensity. On day 7, a significant number of *Oct4*-GFP$^+$CD45$^-$ cells (one-half to two-thirds of total surviving cells) constituted a distinct population from the *Oct4*-GFP$^-$CD45$^-$ cells (Fig. 1c, top, day 7, and Fig. 1d). No obvious generation of *Oct4*-GFP$^+$CD45$^-$ populations was seen in non-treated CD45$^+$ cells cultured similarly but without low-pH treatment (Fig. 1c, bottom).

Low-pH-treated CD45$^+$ cells, but not untreated cells, gradually turned on GFP signals over the first few days (Fig. 1e, Supplementary Videos 1 and 2 and Extended Data Fig. 2a), whereas CD45 immunoreactivity became gradually reduced in the cells that demonstrated *Oct4*-GFP expression (Fig. 1f and Extended Data Fig. 2b). By day 5, the *Oct4*-GFP$^+$ cells attached together and formed clusters by accretion. These GFP$^+$ clusters (but not GFP$^-$ cells) were quite mobile and often showed cell

processes on moving (Supplementary Video 1).

The *Oct4*-GFP$^+$ cells demonstrated a characteristic small cell size with little cytoplasm and also showed a distinct fine structure of the nucleus compared with that of parental CD45$^+$ lymphocytes (Fig. 1g). The *Oct4*-GFP$^+$ cells on day 7 were smaller than non-treated CD45$^+$ cells (Fig. 1g, h and Extended Data Fig. 2c) and embryonic stem (ES) cells (Fig. 1h), both of which are generally considered to be small in size. The diameter of low-pH-treated CD45$^+$ cells became reduced during the first 2 days, even before they started *Oct4*-GFP expression (Fig. 1f), whereas the onset of GFP expression was not accompanied by cell divisions. Consistent with this, no substantial 5-ethynyl-2′-deoxyuridine (EdU) uptake was observed in the *Oct4*-GFP$^+$ cells after the stressor (Extended Data Fig. 2d).

The lack of substantial proliferation argues against the possibility that CD45$^-$ cells, contaminating as a very minor population in the FACS-sorted CD45$^+$ cells, quickly grew and formed a substantial *Oct4*-GFP$^+$ population over the first few days after the low-pH treatment. In addition, genomic rearrangements of *Tcrb* (T-cell receptor gene) were observed in *Oct4*-GFP$^+$ cells derived from FACS-purified CD45$^+$ cells and CD90$^+$CD45$^+$ T cells (Fig. 1i, lanes 4, 5, and Extended Data Fig. 2e–g), indicating at least some contribution from lineage-committed T cells. Thus, *Oct4*-GFP$^+$ cells were generated *de novo* from low-pH-treated CD45$^+$ haematopoietic cells by reprogramming, rather than by simple selection of stress-enduring cells[23].

Low-pH-induced Oct4$^+$ cells have pluripotency

On day 7, the *Oct4*-GFP$^+$ spheres expressed pluripotency-related marker proteins[22] (Oct4, SSEA1, Nanog and E-cadherin; Fig. 2a) and marker genes (*Oct4*, *Nanog*, *Sox2*, *Ecat1* (also called *Khdc3*), *Esg1* (*Dppa5a*), *Dax1* (*Nrob1*) and *Rex1* (*Zfp42*); Fig. 2b and Extended Data Fig. 3a) in a manner comparable to those seen in ES cells[24]. Moderate levels of expression of these pluripotency marker genes were observed on day 3 (Fig. 2b and Extended Data Fig. 3b). Notably, the *Oct4*-GFP$^+$ cells on day 3, but not on day 7, expressed early haematopoietic marker genes such as *Flk1* (also called *Kdr*) and *Tal1* (Extended Data Fig. 3c), indicating that *Oct4*-GFP$^+$ cells on day 3, as judged by their expression pattern at the population level, were still in a dynamic process of conversion.

Figure 2: Low-pH-induced *Oct4*-GFP$^+$ cells represent pluripotent cells.

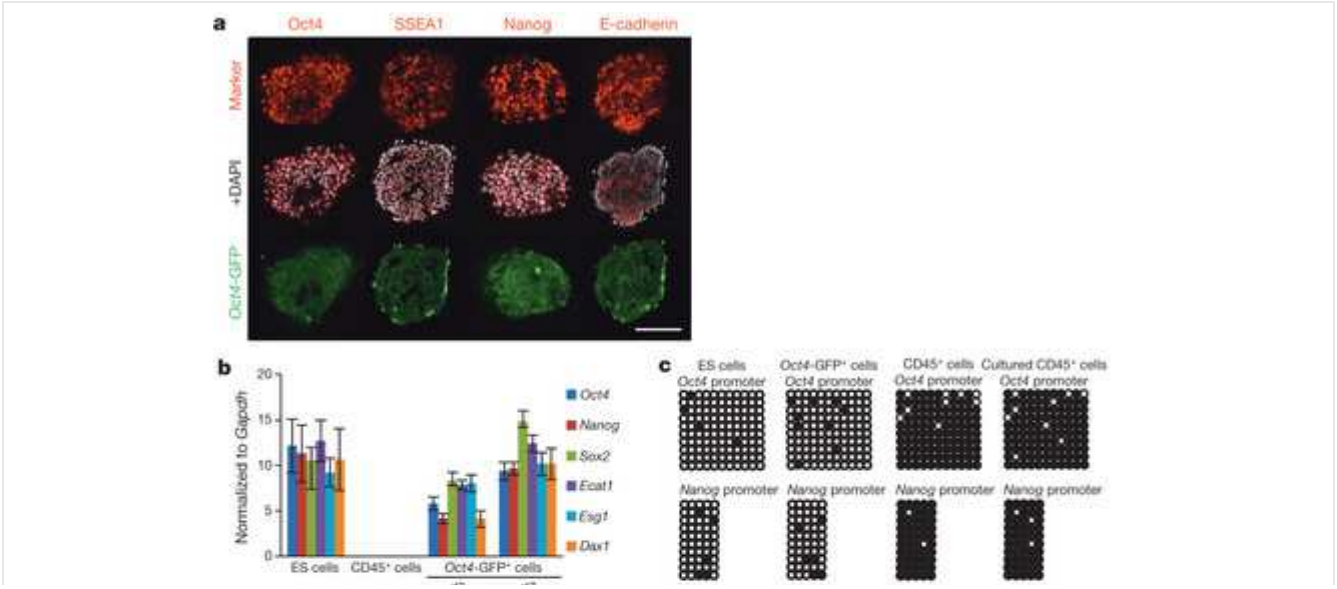

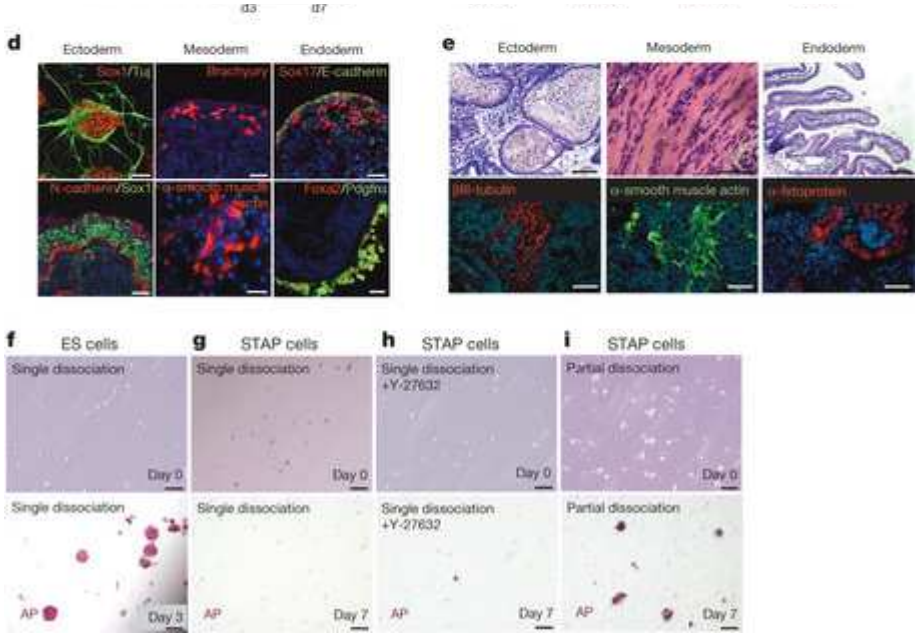

a, Immunostaining for pluripotent cell markers (red) in day 7 *Oct4*-GFP$^+$ (green) clusters. DAPI, white. Scale bar, 50μm. **b**, qPCR analysis of pluripotency marker genes. From left to right, mouse ES cells; parental CD45$^+$ cells; low-pH-induced *Oct4*-GFP$^+$ cells on day 3; low-pH-induced *Oct4*-GFP$^+$ cells on day 7. *n* = 3; error bars show average±s.d. **c**, DNA methylation study by bisulphite sequencing. Filled and open circles indicate methylated and non-methlylated CpG, respectively. **d**, Immunostaining analysis of *in vitro* differentiation capacity of day 7 *Oct4*-GFP$^+$ cells. Ectoderm: the neural markers Sox1/Tuj1 (100%, *n* = 8) and N-cadherin (100%, *n* = 5). Mesoderm: smooth muscle actin (50%, *n* = 6) and brachyury (40%, *n* = 5). Endoderm: Sox17/E-cadherin (67%, *n* = 6) and Foxa2/Pdgfrα (67%, *n* = 6). Scale bar, 50μm. **e**, Teratoma formation assay of day 7 clusters of *Oct4*-GFP$^+$ cells. Haematoxylin and eosin staining showed keratinized epidermis (ectoderm), skeletal muscle (mesoderm) and intestinal villi (endoderm), whereas immunostaining showed expression of Tuj1 (neurons), smooth muscle actin and α-fetoprotein. Scale bar, 100μm. **f**–**i**, Dissociation culture of ES cells and STAP cells (additional 7 days from day 7; **f**, **g**) on gelatin-coated dishes. Top, bright-field; bottom, alkaline phosphatase (AP) staining. Partially dissociated STAP cells slowly generated small colonies (**i**), whereas dissociated STAP cells did not, even in the presence of the ROCK inhibitor (**g**, **h**), which allows dissociation culture of EpiSCs[29].

On day 7, unlike CD45$^+$ cells and like ES cells, low-pH-induced *Oct4*-GFP$^+$ cells displayed extensive demethylation at the *Oct4* and *Nanog* promoter areas (Fig. 2c), indicating that these cells underwent a substantial reprogramming of epigenetic status in these key genes for pluripotency.

In vitro differentiation assays[25, 26, 27] demonstrated that low-pH-induced *Oct4*-GFP$^+$ cells gave rise to three-germ-layer derivatives (Fig. 2d) as well as visceral endoderm-like epithelium (Extended Data Fig. 3d). When grafted into mice, low-pH-induced *Oct4*-GFP$^+$ cell clusters formed teratomas (40%, *n* = 20) (Fig. 2e and Extended Data Fig. 4a–c) but no teratocarcinomas that persistently contained *Oct4*-GFP$^+$ cells (*n* = 50). Because some cellular variation was observed in the signal levels of *Oct4*-GFP within the clusters, we sorted GFP-strong cells (a major population) and GFP-dim cells (a minor population) by FACS on day 7 and separately injected them into mice. In this case, only GFP-strong cells formed teratomas (Extended Data Fig. 4d). In quantitative polymerase chain reaction (qPCR) analysis, the GFP-strong population expressed pluripotency marker genes but not early lineage-specific marker genes, whereas the GFP-dim cells showed substantial expression of some early lineage-specific

marker genes (*Flk1*, *Gata2*, *Gata4*, *Pax6* and *Sox17*; Extended Data Fig. 4e) but not *Nanog* and *Rex1*. These observations indicate that three-germ-layer derivatives were generated from the GFP-strong cells expressing pluripotency marker genes, rather than from GFP-dim cells that seem to contain partially reprogrammed cells.

Collectively, these findings show that the differentiation state of a committed somatic cell lineage can be converted into a state of pluripotency by strong stimuli given externally. Hereafter, we refer to the fate conversion from somatic cells into pluripotent cells by strong external stimuli such as low pH as 'stimulus-triggered acquisition of pluripotency' (STAP) and the resultant cells as STAP cells. Under their establishment conditions, these STAP cells were rarely proliferative (Extended Data Figs 2d and 5a, b). Comparative genomic hybridization array analysis of STAP cells indicated no major global changes in chromosome number (Extended Data Fig. 5c).

STAP cells compared to ES cells

STAP cells, unlike mouse ES cells, showed a limited capacity for self-renewal in the LIF-containing medium and did not efficiently form colonies in dissociation culture (Fig. 2f, g), even in the presence of the ROCK inhibitor Y-27632, which suppresses dissociation-induced apoptosis[28, 29] (Fig. 2h). Also, even under high-density culture conditions after partial dissociation (Fig. 2i), STAP cell numbers started to decline substantially after two passages. Furthermore, expression of the ES cell marker protein Esrrβ was low in STAP cells (Extended Data Fig. 5d, e). In general, female ES cells do not show X-chromosomal inactivation[30] and contain no H3K27me3-dense foci (indicative of inactivated X chromosomes), unlike female CD45$^+$ cells and EpiSCs. In contrast, H3K27me3-dense foci were found in ~40% of female STAP cells strongly positive for *Oct4*-GFP (Extended Data Fig. 5f, g).

STAP cells were also dissimilar to mouse EpiSCs, another category of pluripotent stem cell[21, 22, 29, 31], and were positive for Klf4 and negative for the epithelial tight junction markers claudin 7 and ZO-1 (Extended Data Fig. 5d, e).

STAP cells from other tissue sources

We next performed similar conversion experiments with somatic cells collected from brain, skin, muscle, fat, bone marrow, lung and liver tissues of 1-week-old *Oct4-gfp* mice. Although conversion efficacy varied, the low-pH-triggered generation of *Oct4*-GFP$^+$ cells was observed in day 7 culture of all tissues examined (Fig. 3a and Extended Data Fig. 6a–c), including mesenchymal cells of adipose tissues (Fig. 3a–c) and neonatal cardiac cells that were negatively sorted for CD45 by FACS (Fig. 3d–g; see Extended Data Fig. 6d for suppression of cardiac genes such as *Nkx2-5* and cardiac actin).

Figure 3: STAP cell conversion from a variety of cells by low-pH treatment.

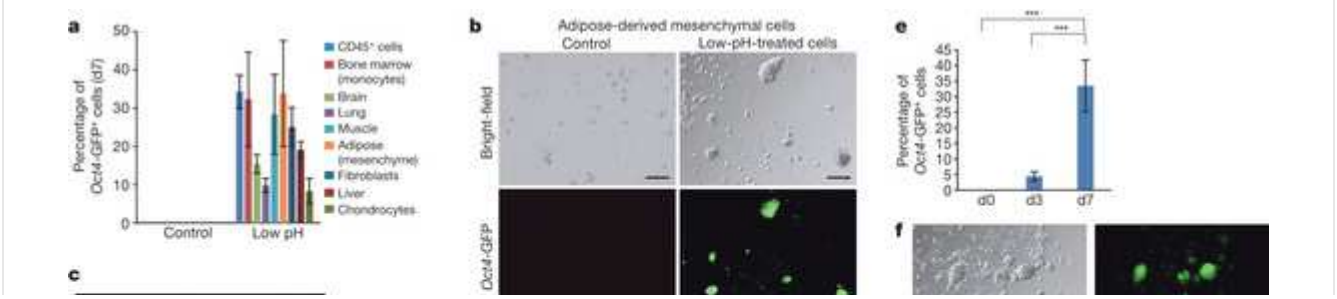

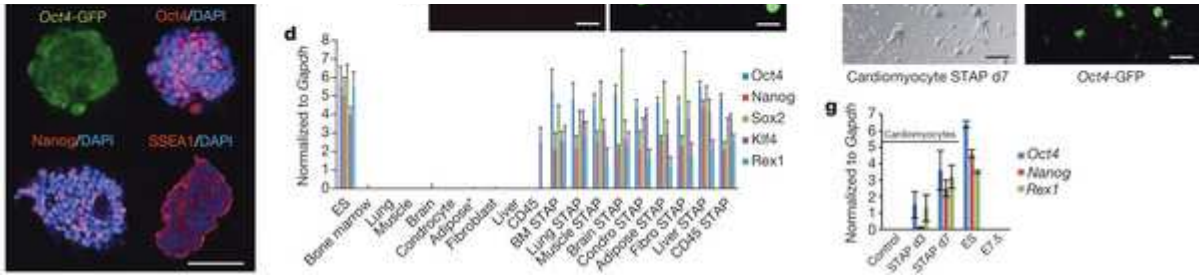

a, Percentage of *Oct4*-GFP$^+$ cells in day 7 culture of low-pH-treated cells from different origins (1×10^5 cells per ml×3 ml). The number of surviving cells on day 7 compared to the plating cell number was 20–30%, except for lung, muscle and adipose cells, for which surviving cells were ~10% (n = 3, average±s.d.). **b**, *Oct4*-GFP$^+$ cell clusters were induced by low-pH treatment from adipose-tissue-derived mesenchymal cells on day 7. Scale bar, 100 µm. **c**, Expression of pluripotent cell markers in day 7 clusters of low-pH-treated adipose-tissue-derived mesenchymal cells. Scale bar, 50 µm. **d**, Expression of pluripotency marker genes in STAP cells derived from various tissues. Gene expressions were normalized by *Gapdh* (n = 3, average±s.d.). Asterisk indicates adipose tissue-derived mesenchymal cells. **e**, Quantification of *Oct4*-GFP$^+$ cells in culture of low-pH-treated neonatal cardiac muscle cells. ***P<0.001; Tukey's test (n = 3). **f**, Generation of *Oct4*-GFP$^+$ cell clusters (d7) from CD45$^-$ cardiac muscle cells. **g**, qPCR analysis of pluripotency marker genes in STAP cells from CD45$^-$ cardiac muscle cells.

Chimaera formation and germline transmission in mice

We next performed a blastocyst injection assay with STAP cells that were generated from CD45$^+$ cells of neonatal mice constitutively expressing GFP (this C57BL/6 line with *cag-gfp* transgenes is referred to hereafter as B6GFP). We injected STAP cell clusters en bloc that were manually cut into small pieces using a microknife (Fig. 4a). A high-to-moderate contribution of GFP-expressing cells was seen in the chimaeric embryos (Fig. 4b and Extended Data Fig. 7a). These chimaeric mice were born at a substantial rate and all developed normally (Fig. 4c and Extended Data Fig. 7b).

Figure 4: Chimaeric mouse generation from STAP cells.

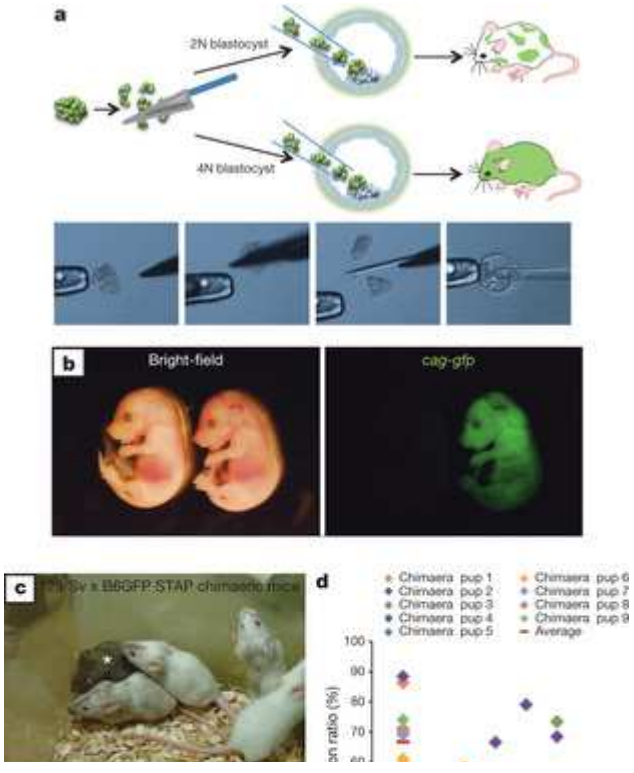

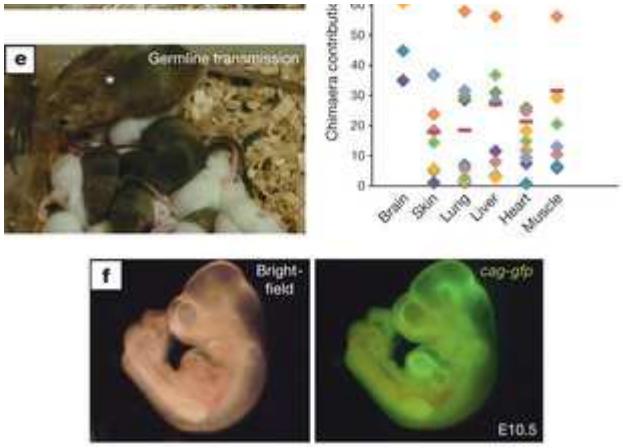

a, Schematic of chimaeric mouse generation. **b**, E13.5 chimaera fetuses from 2N blastocytes injected with STAP cells (derived from B6GFP CD45$^+$ cells carrying *cag-gfp*). **c**, Adult chimaeric mice generated by STAP-cell (B6GFP × 129/Sv; agouti) injection into blastocysts (ICR strain; albino). Asterisk indicates a highly contributed chimaeric mouse. **d**, Chimaera contribution analysis. Tissues from nine pups were analysed by FACS. **e**, Offspring of chimaeric mice derived from STAP cells. Asterisk indicates the same chimaeric mouse shown in **c**. **f**, E10.5 embryo generated in the tetraploid complementation assay with STAP cells (B6GFP × 129/Sv).

CD45$^+$ cell-derived STAP cells contributed to all tissues examined (Fig. 4d). Furthermore, offspring derived from STAP cells were born to the chimaeric mice (Fig. 4e and Extended Data Fig. 7c), demonstrating their germline transmission, which is a strict criterion for pluripotency as well as genetic and epigenetic normality[32, 33]. Furthermore, in a tetraploid (4N) complementation assay, which is considered to be the most rigorous test for developmental potency[34, 35] (Fig. 4a, bottom), CD45$^+$ cell-derived STAP cells (from F_1 mice of B6GFP × 129/Sv or DBA/2) generated all-GFP$^+$ embryos on embryonic day (E)10.5 (Fig. 4f, Extended Data Fig. 7d and Supplementary Video 3), demonstrating that STAP cells alone are sufficient to construct an entire embryonic structure. Thus, STAP cells have the developmental capacity to differentiate into all somatic-cell lineages as well as germ-cell lineages *in vivo*.

Expandable pluripotent cell lines from STAP cells

STAP cells have a limited self-renewal capacity under the conditions used for establishment (Fig. 2g and Extended Data Figs 2e and 5a). However, in the context of the embryonic environment, a small fragment of a STAP cell cluster could grow even into a whole embryo (Fig. 4f). With this in mind, we next examined whether STAP cells have the potential to generate expandable pluripotent cell lines *in vitro* under certain conditions.

STAP cells could not be efficiently maintained for additional passages in conventional LIF+FBS-containing medium or 2i medium[20] (most STAP cells died in 2i medium within 7 days; Extended Data Fig. 8a). Notably, an adrenocorticotropic hormone (ACTH)+LIF-containing medium (hereafter called ACTH medium) known to facilitate clonal expansion of ES cells[36] supported outgrowth of STAP cell colonies. When cultured in this medium on a MEF feeder or gelatin, a portion of STAP cell clusters started to grow (Fig. 5a, bottom; such outgrowth was typically found in 10–20% of wells in single cluster culture using 96-well plates and in >75% when 12 clusters were plated per well). These growing

colonies looked similar to those of mouse ES cells and expressed a high level of *Oct4*-GFP.

Figure 5: ES-cell-like stem cells can be derived from STAP cells.

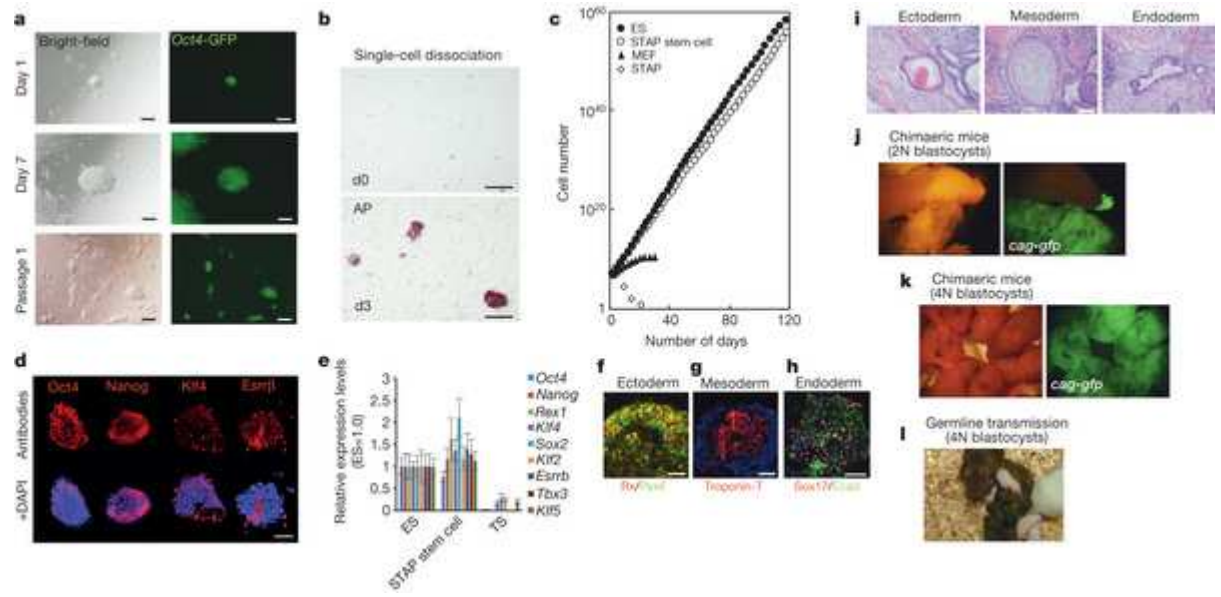

a, Growth of STAP stem cells carrying *Oct4-gfp*. Scale bar, 50 μm. **b**, Dissociation culture of STAP stem cells to form colonies. Scale bar, 100 μm. **c**, Robust growth of STAP stem cells in maintenance culture. Similar results were obtained with eight independent lines. In contrast, parental STAP cells decreased in number quickly. **d**, Immunostaining of STAP stem cells for pluripotency markers (red). Scale bar, 50 μm. **e**, qPCR analysis of pluripotency marker gene expression. **f**–**h**, *In vitro* differentiation assays into three-germ-layer derivatives. **f**, Ectoderm: $Rx^{+}/Pax6^{+}$ (retinal epithelium; 83%, $n = 6$). **g**, Mesoderm: troponin-T^{+} (cardiac muscle; 50%, $n = 6$). **h**, Endoderm: $Sox17^{+}$/E-cadherin^{+} (endodermal progenitors; 67%, $n = 6$). Scale bar, 50 μm. **i**, Teratoma formation assays. Formation of keratinized epidermis (ectoderm; left), cartilage (mesoderm; middle) and bronchial-like epithelium (endoderm; right) is shown. Scale bar, 100 μm. **j**, Blastocyst injection assays. These pictures of live animals were taken serially (asterisk indicates the same chimaeric pup). **k**, **l**, Tetraploid complementation assay. 'All-GFP^{+}' pups were born (**k**) and germline transmission was observed (**l**).

After culturing in ACTH medium for 7 days, this growing population of cells, unlike parental STAP cells, could be passaged as single cells (Fig. 5a, bottom, and Fig. 5b), grow in 2i medium (Extended Data Fig. 8a) and expand exponentially, up to at least 120 days of culture (Fig. 5c; no substantial chromosomal abnormality was seen; Extended Data Fig. 8b, c). Hereafter, we refer to the proliferative cells derived from STAP cells as STAP stem cells.

STAP stem cells expressed protein and RNA markers for pluripotent cells (Fig. 5d, e), showed low DNA methylation levels at the *Oct4* and *Nanog* loci (Extended Data Fig. 8d), and had a nuclear fine structure similar to that of ES cells (Extended Data Fig. 8e; few electron-dense areas corresponding to heterochromatin). In differentiation culture[25, 26, 27], STAP stem cells generated ectodermal, mesodermal and endodermal derivatives *in vitro* (Fig. 5f–h and Extended Data Fig. 8f, g), including beating cardiac muscles (Supplementary Video 4), and formed teratomas *in vivo* (Fig.5i and Extended Data Fig. 8h; no teratocarcinomas, $n = 40$). After blastocyst injection, STAP stem cells efficiently contributed to chimaeric mice (Fig. 5j), in which germline transmission was seen (Extended Data Fig. 8i). Even in tetraploid complementation assays, injected STAP stem cells could generate mice capable

of growing to adults and producing offspring (Fig. 5k, l; in all eight independent lines, Extended Data Fig. 8j).

In addition to their expandability, we noticed at least two other differences between STAP stem cells and parental STAP cells. First, the expression of the ES cell marker protein Esrrβ, which was undetectable in STAP cells (Extended Data Fig. 5d, e), was clearly seen in STAP stem cells (Fig. 5e). Second, the presence of H3K27me3 foci, which was found in a substantial proportion of female STAP cells, was no longer observed in STAP stem cells (Extended Data Figs 5f and 8k). Thus, STAP cells have the potential to give rise to expandable cell lines that exhibit features similar to those of ES cells.

Discussion

This study has revealed that somatic cells latently possess a surprising plasticity. This dynamic plasticity—the ability to become pluripotent cells—emerges when cells are transiently exposed to strong stimuli that they would not normally experience in their living environments.

Low-pH treatment was also used in the 'autoneuralization' experiment[15, 16, 17] by Holtfreter in 1947, in which exposure to acidic medium caused tissue-autonomous neural conversion of salamander animal caps *in vitro* in the absence of Spemann's organizer signals. Although the mechanism has remained elusive, Holtfreter hypothesized that the strong stimulus releases the animal cap cells from some intrinsic inhibitory mechanisms that suppress fate conversion or, in his words, they pass through 'sublethal cytolysis' (meaning stimulus-evoked lysis of the cell's inhibitory state)[15, 37]. Although Holtfreter's study and ours differ in the direction of fate conversion—orthograde differentiation and nuclear reprogramming, respectively—these phenomena may share some common aspects, particularly with regard to sublethal stimulus-evoked release from a static (conversion-resisting) state in the cell.

A remaining question is whether cellular reprogramming is initiated specifically by the low-pH treatment or also by some other types of sublethal stress such as physical damage, plasma membrane perforation, osmotic pressure shock, growth-factor deprivation, heat shock or high Ca^{2+} exposure. At least some of these stressors, particularly physical damage by rigorous trituration and membrane perforation by streptolysin O, induced the generation of *Oct4*-GFP^{+} cells from CD45^{+} cells (Extended Data Fig. 9a; see Methods). These findings raise the possibility that certain common regulatory modules, lying downstream of these distantly related sublethal stresses, act as a key for releasing somatic cells from the tightly locked epigenetic state of differentiation, leading to a global change in epigenetic regulation. In other words, unknown cellular functions, activated by sublethal stimuli, may set somatic cells free from their current commitment to recover the naive cell state.

Our present finding of an unexpectedly large capacity for radical reprogramming in committed somatic cells raises various important questions. For instance, why, and for what purpose, do somatic cells latently possess this self-driven ability for nuclear reprogramming, which emerges only after sublethal stimulation, and how, then, is this reprogramming mechanism normally suppressed? Furthermore, why isn't teratoma (or pluripotent cell mass) formation normally seen in *in vivo* tissues that may receive strong environmental stress? In our preliminary study, experimental reflux oesophagitis locally induced

moderate expression of *Oct4*-GFP but not endogenous Nanog in the mouse oesophageal mucosa (Extended Data Fig. 9b). Therefore, an intriguing hypothesis for future research is that the progression from initial *Oct4* activation to further reprogramming is suppressed by certain inhibitory mechanisms *in vivo*.

The question of why and how this self-driven reprogramming is directed towards the pluripotent state is fundamentally important, given that STAP reprogramming takes a remarkably short period, only a few days for substantial expression of pluripotency marker genes, unlike transgene- or chemical-induced iPS cell conversion[38]. Thus, our results cast new light on the biological meaning of diverse cellular states in multicellular organisms.

Methods

Animal studies

Research involving animals complied with protocols approved by the Harvard Medical School/Brigham and Women's Hospital Committee on Animal Care, and the Institutional Committee of Laboratory Animal Experimentation of the RIKEN Center for Developmental Biology.

Tissue collection and low-pH treatment

To isolate $CD45^+$ haematopoietic cells, spleens were excised from 1-week-old *Oct4-gfp* mice (unless specified otherwise), minced by scissors and mechanically dissociated with pasture pipettes. Dissociated spleen cells were suspended with PBS and strained through a cell strainer (BD Biosciences). After centrifuge at 1,000 r.p.m. for 5 min, collected cells were re-suspended in DMEM medium and added to the same volume of lympholyte (Cedarlane), then centrifuged at 1,000*g* for 20 min. The lymphocyte layer was taken out and stained with CD45 antibody (ab25603, Abcam). CD45-positive cells were sorted by FACS Aria (BD Biosciences). After cell sorting, 1×10^6 CD45-positive cells were treated with 500 µl of low-pH HBSS solution (titrated to pH5.7 by HCl) for 25 min at 37 °C, and then centrifuged at 1,000 r.p.m. at room temperature for 5 min. After the supernatant (low-pH solution) was removed, precipitated cells were re-suspended and plated onto non-adhesive culture plates (typically, 1×10^5 cells ml^{-1}) in DMEM/F12 medium supplemented with 1,000 U LIF (Sigma) and 2% B27 (Invitrogen). Cell cluster formation was more sensitive to the plating cell density than the percentage of *Oct4*-GFP^+ cells. The number of surviving cells was sensitive to the age of donor mice and was low under the treatment conditions above when adult spleens were used. The addition of LIF during days 2–7 was essential for generating *Oct4*-GFP^+ STAP cell clusters on day 7, as shown in Extended Data Fig. 1f. Even in the absence of LIF, *Oct4*-GFP^+ cells (most of them were dim in signal) appeared transiently during days 2–5 in culture of low-pH-treated $CD45^+$ cells, but subsequently disappeared, indicating that there is a LIF-independent early phase, whereas the subsequent phase is LIF-dependent.

Chimaeric mouse generation and analyses

For production of diploid and tetraploid chimaeras with STAP cells, diploid embryos were obtained from ICR strain females. Tetraploid embryos were produced by electrofusion of 2-cell embryos. Because trypsin treatment of donor samples turned out to cause low chimaerism, STAP spherical colonies were cut into small pieces using a microknife under the microscope, and small clusters of STAP cells were

then injected into day-4.5 blastocysts by a large pipette. The next day, the chimaeric blastocysts were transferred into day-2.5 pseudopregnant females. For experiments using STAP cells from $CD45^+$ cells without the *Oct4-gfp* reporter, STAP cell clusters were identified by their characteristic cluster morphology (they are made of very small cells with no strong compaction in the aggregate). When the STAP conversion conditions (low pH) were applied to $CD45^+$ lymphocytes, most day-7 clusters that were large and contained more than a few dozen small cells were positive for Oct4 (although the expression level varied). Therefore, we used only well-formed characteristic clusters (large ones) for this type of study and cut them by microknife to prepare donor cell clusters in a proper size for glass needle injection. For an estimate of the contribution of these injected cells, we used STAP cells that were generated from $CD45^+$ cells of mice constitutively expressing GFP (C57BL/6 line with *cag-gfp* transgenes; F_1 of C57BL/6 and 129/Sv or DBA/2 was used from the viewpoint of heterosis).

Because the number of $CD45^+$ cells from a neonatal spleen was small, we mixed spleen cells from male and female mice for STAP cell conversion. To make germline transmission more efficient, we intercrossed chimaeras in some experiments.

For the production of diploid and tetraploid chimaeras with STAP stem cells, diploid embryos were obtained from ICR strain females. Tetraploid embryos were produced by electrofusion of 2-cell embryos. STAP stem cells were dissociated into single cells and injected into day-4.5 blastocysts. In the chimaera studies with both STAP cells and STAP stem cells, we did not find tumorigenetic tendencies in their chimaeras or their offspring (up to 18 months).

***In vivo* differentiation assay**

1×10^7 STAP cells were seeded onto a sheet composed of a non-woven mesh of polyglycolic acid fibres (3× 3×1 mm; 200 μm in pore diameter), cultured for 24 h in DMEM + 10% FBS, and implanted subcutaneously into the dorsal flanks of 4-week-old mice. In this experiment, to better support tumour formation from slow growing STAP cells by keeping cells in a locally dense manner, we implanted STAP cells with artificial scaffold made of polyglycolic acid fibres. Given the artificial nature of the material, we used NOD/SCID mice as hosts, to avoid possible enhancement of post-graft inflammation caused by this scaffold even in syngenic mice. STAP stem cells were dissociated into single cells and cell suspension containing 1×10^7 cells was injected into the testis. Six weeks later, the implants were analysed using histochemical techniques. The implants were fixed with 10% formaldehyde, embedded in paraffin, and routinely processed into 4-μm-thick sections. Sections were stained with haematoxylin and eosin. Endoderm tissues were identified with expression of anti-α-fetoprotein (mouse monoclonal antibody; MAB1368, R&D Systems). Ectodermal tissues were identified with expression of anti-βIII tubulin (mouse monoclonal antibody; G7121, Promega). Mesodermal tissues were identified with expression of anti-α-smooth muscle actin (rabbit polyclonal; DAKO). In negative controls, the primary antibody was replaced with IgG-negative controls of the same isotype to ensure specificity.

STAP by exposure to other external stimuli

To give a mechanical stress to mature cells, a pasture pipette was heated and then stretched to create thin capillaries with the lumens approximately 50 μm in diameter, and then broken into appropriate lengths. Mature somatic cells were then repeatedly triturated through these pipettes for 20 min, and then

cultured for 7 days. To provide a heat shock, cells were heated at 42 °C for 20 min and cultured for 7 days. A nutrition-deprivation stress was provided to mature cells, by culturing the cells in basal culture medium for 3 weeks. High Ca^{2+} concentration stress was provided to mature cells by culturing cells in medium containing 2 mM $CaCl_2$ for 7 days. To give a strong stress by creating pores in cell membranes, cells were treated with 230 ng ml^{-1} streptolysine O (SLO) (S5265, Sigma) for 2 h, then cultured for 7 days. After each treatment, the ratio of *Oct4*-GFP-positive cells was analysed by FACS.

Bisulphite sequencing

GFP-positive cells in STAP clusters were collected by FACS Aria. Genomic DNA was extracted from STAP cells and analysed. Bisulphite treatment of DNA was performed using the CpGenome DNA modification kit (Chemicon, http://www.chemicon.com), following the manufacturer's instructions. The resulting modified DNA was amplified by nested PCR using two forward (F) primers and one reverse (R) primer: Oct4 (F1, 5′-GTTGTTTTGTTTTGGTTTTGGATAT-3′; F2, 5′-ATGGGTTGAAATATTGGGTTTATTTA-3′; R, 5′-CCACCCTCTAACCTTAACCTCTAAC-3′). And Nanog (F1, 5′-GAGGATGTTTTTTAAGTTTTTTTT-3′; F2, 5′-AATGTTTATGGTGGATTTTGTAGGT-3′; R, 5′-CCCACACTCATATCAATATAATAAC-3′). PCR was done using TaKaKa Ex Taq Hot Start Version (RR030A). DNA sequencing was performed using a M13 primer at the Genome Resource and Analysis Unit, RIKEN CDB.

Immunohistochemistry

Cultured cells were fixed with 4% paraformaldehyde and permeabilized with 0.1% Triton X-100/PBS before blocking with 1% BSA solution. Cells were incubated with the following primary antibodies: anti-Oct4 (Santa Cruz Biotechnology; C-10), anti-Nanog (eBioscience; MLC-51), anti-SSEA-1 (Millipore; MC480), anti-E-cadherin (Abcam), anti-ZO-1 (Santa Cruz Biotechnology; c1607), anti-claudin7 (Abcam), anti-Klf4 (R&D Systems), anti-Esrrβ (R&D Systems), anti-H3K27me3 (Millipore), anti-BrdU (BD Bioscience) and anti-Ki67 (BD Pharmingen). After overnight incubation, cells were incubated with secondary antibodies: goat anti-mouse or -rabbit coupled to Alexa-488 or -594 (Invitrogen). Cell nuclei were visualized with DAPI (Sigma). Slides were mounted with a SlowFade Gold antifade reagent (Invitrogen).

Fluorescence-activated cell sorting and flow cytometry

Cells were prepared according to standard protocols and suspended in 0.1% BSA/PBS on ice before FACS. Propidium iodide (BD Biosciences) was used to exclude dead cells. In negative controls, the primary antibody was replaced with IgG-negative controls of the same isotype to ensure specificity. Cells were sorted on a BD FACSAria SORP and analysed on a BD LSRII with BD FACS Diva Software (BD Biosciences). For haematopoietic fraction sorting, antibodies against T-cell marker (anti-CD90; eBioscience), B-cell marker (anti-CD19; Abcam) and haematopoietic progenitor marker (anti-CD34; Abcam) were used.

RNA preparation and RT–PCR analysis

RNA was isolated with the RNeasy Micro kit (Qiagen). Reverse transcription was performed with the SuperScript III first strand synthesis kit (Invitrogen). Power SYBR Green Mix (Roche Diagnostics) was used for amplification, and samples were run on a Lightcycler-II Instrument (Roche Diagnostics). The

primer sets for each gene are listed in Supplementary Table 1.

In vitro differentiation assays

For mesodermal differentiation assay, STAP cells were collected at 7 days, and *Oct4*-GFP-positive cells were collected by cell sorter and subjected to culture in DMEM supplemented with 20% FBS. Medium was exchanged every 3 days. After 7–14 days, muscle cells were stained with an anti-α-smooth muscle actin antibody (DAKO).

For neural lineage differentiation assay, STAP cells were collected at 7 days and subjected to SDIA or SFEBq culture. For SDIA culture, collected STAP cell clusters were plated on PA6 cell feeder as described previously[26]. For SFEBq culture, STAP cell clusters (one per well; non-cell-adhesive 96-well plate, PrimeSurface V-bottom, Sumitomo Bakelite) were plated and cultured in suspension as described previously[36].

For endodermal differentiation, STAP cells were collected at 7 days and subjected to suspension culture with inducers in 96-well plates[27].

TCR-β chain gene rearrangement analysis

Genomic DNA was extracted from STAP cells and tail tips from chimaeric mice generated with STAP cells derived from $CD45^+$ cells. PCR was performed with 50 ng DNA using the following primers (Dβ2: 5′-GCACCTGTGGGGAAGAAACT-3′ and Jβ2.6: 5′-TGAGAGCTGTCTCCTACTATCGATT-3′) that amplify the regions of the (D)J recombination. The PCR products were subjected to gel electrophoresis in Tris-acetate-EDTA buffer with 1.6% agarose and visualized by staining with ethidium bromide. PCR bands from STAP cells were subjected to sequencing analysis and identified as rearranged genomic fragments of the (D)J recombination.

EdU uptake assay and apoptosis analysis

At various phases in STAP cell culture (days 0–2, 2–7, 7–14), EdU was added to the culture medium (final concentration: 10 μM) and EdU uptake was analysed by FACS. This assay was performed according to the manufacturer's protocol with the Click-iT EdU Flow cytometry assay kit (Invitrogen).

Apoptosis analysis was performed with flow cytometry using Annexin-V (Biovision) and propidium iodide. Annexin-V analysis by FACS on day 14 showed that most *Oct4*-GFP^+ cells were positive for this apoptotic marker; indeed, the number of surviving cells declined thereafter.

Soft agar assay

Sorted STAP cells (*Oct4*-GFP-strong or -dim) and control mouse ES cells (1,000 cells per well of 96-well plate) were plated into soft ager medium (0.4% agarose) in LIF-B27 medium. After 7 days of culture, cells were dissociated and their anchorage-independent growth was quantified by fluorescent measurement with the cytoselect 96-well cell transformation assay kit (Cell Biolabs) according to the manufacturer's protocol.

Comparative genomic hybridization (CGH) array analysis

Genomic DNA was extracted from STAP (male) and CD45-positive cells (male) by the Gene JET Genomic DNA purification kit (Thermo Scientific). Using CGH array (Agilent), the normality of chromosomes derived from STAP was compared with that of CD45-positive cells whose chromosomal normality was confirmed by a separate experiment. CGH array and data analysis were performed at TAKARA Bio.

Electron microscopy

For electron microscopic analysis, dissociated cells were fixed in 2.5% glutaraldehyde and 2% formaldehyde in 0.1 M cacodylate buffer (pH 7.2) and then processed for thin sectioning and transmission electron microscopy.

Live cell imaging

All live-cell imaging was performed with LCV110-CSUW1 (Olympus). For live-cell imaging of 'in culture CD45 antibody staining', $CD45^+$ cells treated with low pH were plated in culture medium containing 20 ng ml^{-1} of fluorescent-labelled CD45 antibody (eBioscience)[40].

RNA-sequencing and ChIP sequencing analyses

For RNA sequencing of cell lines, total RNA was extracted from cells by the RNasy mini kit (Qiagen). RNA-seq libraries were prepared from 1 μg total RNAs following the protocol of the TruSeq RNA Sample Prep kit (Illumina) and subjected to the deep sequencing analysis with Illumina Hi-Seq1500. Cluster tree diagram of various cell types was obtained from hierarchical clustering of global expression profiles ($\log_2$ FPKM of all transcripts; FPKM, fragments per kilobase of transcript per million mapped reads). Complete linkage method applied to $1-r$ (r = Pearson's correlation between profiles) was used for generating the tree and 1,000 cycles of bootstrap resampling were carried out to obtain statistical confidence score in per cent units (also called AU P values).

ChIP-seq libraries were prepared from 20 ng input DNAs, 1 ng H3K4me3 ChIP DNAs, or 5 ng H3K27me3 ChIP DNAs using the KAPA Library Preparation kit (KAPA Biosystems). TruSeq adaptors were prepared in-house by annealing a TruSeq universal oligonucleotide and each of index oligonucleotides (5′-AATGATACGGCGACCACCGAGATCTACACTCTTTCCCTACACGACGCTCTTCCGATCT-3′, and 5′-GATCGGAAGAGCACACGTCTGAACTCCAGTCACXXXXXXATCTCGTATGCCGTCTTCTGCTTG-3′; where X represents index sequences).

Chromatin immunoprecipitation was performed as follows. Cells were fixed in PBS(-) containing 1% formaldehyde for 10 min at room temperature. Glycine was added to a final concentration of 0.25 M to stop the fixation. After washing the cells twice in ice-cold PBS(-), cells were further washed in LB1 (50 mM HEPES-KOH pH 7.5, 140 mM NaCl, 1 mM EDTA, 10% glycerol, 0.5% NP-40, 0.25% Triton X-100) and LB2 (10 mM Tris-HCl pH 8.0, 200 mM NaCl, 1 mM EDTA, 0.5 mM EGTA). Cells were then re-suspended in lysis buffer (50 mM Tris-HCl pH 8.0, 10 mM EDTA, 1% SDS). Lysates were prepared by sonication using Covaris S220 in a mini tube at duty cycle = 5%, PIP = 70, cycles per burst = 200, and the treatment time of 20 min. Lysates from 2×10^6 cells were diluted in ChIP dilution buffer (16.7 mM Tris-HCl pH 8.0, 167 mM NaCl, 1.2 mM EDTA, 1.1% Triton X-100, 0.01% SDS). ChIP was performed

using sheep anti-mouse IgG beads (Invitrogen) or protein A beads (Invitrogen) coupled with anti-histone H3K4me3 antibody (Wako, catalogue no. 307-34813) or anti-histone H3K27me3 antibody (CST, catalogue no. 9733), respectively. After 4–6 h of incubation in a rotator at 4 °C, beads were washed five times in low-salt wash buffer (20 mM Tris HCl pH 8.0, 150 mM NaCl, 2 mM EDTA, 1% Triton X-100, 0.1% SDS), and three times in high-salt wash buffer (20 mM Tris-HCl pH 8.0, 500 mM NaCl, 2 mM EDTA, 1% Triton X-100, 0.1% SDS). Target chromatin was eluted off the beads in elution buffer (10 mM Tris-HCl pH 8.0, 300 mM NaCl, 5 mM EDTA, 1% SDS) at room temperature for 20 min. Crosslink was reversed at 65 °C, and then samples were treated with RNaseA and proteinase K. The prepared DNA samples were purified by phenol-chloroform extraction followed by ethanol precipitation and dissolved in TE buffer.

STAP stem-cell conversion culture

For establishment of STAP stem-cell lines, STAP cell clusters were transferred to ACTH-containing medium[36] on MEF feeder cells (several clusters, up to a dozen clusters, per well of 96-well plates). Four to seven days later, the cells were subjected to the first passage using a conventional trypsin method, and suspended cells were plated in ES maintain medium containing 20% FBS. Subsequent passaging was performed at a split ratio of 1:10 every second day before they reached subconfluency. We tested the following three different genetic backgrounds of mice for STAP stem-cell establishment from STAP cell clusters, and observed reproducible data of establishment: C57BL/6 carrying *Oct4-gfp* (29 of 29), 129/Sv carrying *Rosa26-gfp* (2 of 2) and 129/Sv×C57BL/6 carrying *cag-gfp* (12 of 16). STAP stem cells with all these genetic backgrounds showed chimaera-forming activity.

For clonal analysis of STAP stem cells, single STAP stem cells were manually picked by a thin-glass pipette, and plated into 96-well plates at one cell per well. The clonal colonies were cultured in ES medium containing 20% FBS, and expanded for subsequent experiments.

Karyotype analysis

Karyotype analysis was performed by Multicolor FISH analysis (M-FISH). Subconfluent STAP stem cells were arrested in metaphase by colcemid (final concentration 0.270 μg ml^{-1}) to the culture medium for 2.5 h at 37 °C in 5% CO_2. Cells were washed with PBS, treated with trypsin and EDTA (EDTA), re-suspended into cell medium and centrifuged for 5 min at 1,200 r.p.m. To the cell pellet in 3 ml of PBS, 7 ml of a pre-warmed hypotonic 0.0375 M KC1 solution was added. Cells were incubated for 20 min at 37 °C. Cells were centrifuged for 5 min at 1,200 r.p.m. and the pellet was re-suspended in 3–5 ml of 0.0375 M KC1 solution. The cells were fixed with methanol/acetic acid (3:1; vol/vol) by gently pipetting. Fixation was performed four times before spreading the cells on glass slides. For the FISH procedure, mouse chromosome-specific painting probes were combinatorially labelled using seven different fluorochromes and hybridized as previously described[41]. For each cell line, 9–15 metaphase spreads were acquired by using a Leica DM RXA RF8 epifluorescence microscope (Leica Mikrosysteme GmbH) equipped with a Sensys CCD camera (Photometrics). Camera and microscope were controlled by the Leica Q-FISH software (Leica Microsystems). Metaphase spreads were processed on the basis of the Leica MCK software and presented as multicolour karyograms.

Q-band analysis was performed at Chromocentre (Japan). After quinacrin staining, 20 cells from each sample were randomly selected and the normality of chromosomes was analysed. Five different

independent lines of STAP stem cells showed no chromosomal abnormalities in Q-band analysis after >10 passages.

References

1. Gurdon, J. B. The developmental capacity of nuclei taken from intestinal epithelium cells of feeding tadpoles. *J. Embryol. Exp. Morphol.* **10**, 622–640 (1962)
2. Wakayama, T., Perry, A. C., Zuccotti, M., Johnson, K. R. & Yanagimachi, R. Full-term development of mice from enucleated oocytes injected with cumulus cell nuclei. *Nature* **394**, 369–374 (1998)
3. Takahashi, K. & Yamanaka, S. Induction of pluripotent stem cells from mouse embryonic and adult fibroblast cultures by defined factors. *Cell* **126**, 663–676 (2006)
4. Thorpe, T. A. History of plant tissue culture. *Mol. Biotechnol.* **37**, 169–180 (2007)
5. Jiang, Y. *et al.* Pluripotency of mesenchymal stem cells derived from adult marrow. *Nature* **418**, 41–49 (2002)
6. D'Ippolito, G. *et al.* Marrow-isolated adult multilineage inducible (MIAMI) cells, a unique population of postnatal young and old human cells with extensive expansion and differentiation potential. *J. Cell Sci.* **117**, 2971–2981 (2004)
7. Kucia, M. *et al.* A population of very small embryonic-like (VSEL) $CXCR4^{+}SSEA\text{-}1^{+}Oct\text{-}4^{+}$ stem cells identified in adult bone marrow. *Leukemia* **20**, 857–869 (2006)
8. Kuroda, Y. *et al.* Unique multipotent cells in adult human mesenchymal cell populations. *Proc. Natl Acad. Sci. USA* **107**, 8639–8643 (2010)
9. Obokata, H. *et al.* The potential of stem cells in adult tissues representative of the three germ layers. *Tissue Eng. Part A* **17**, 607–615 (2011)
10. Lengner, C. J., Welstead, G. G. & Jaenisch, R. The pluripotency regulator Oct4: a role in somatic stem cells? *Cell Cycle* **7**, 725–728 (2008)
11. Berg, J. S. & Goodell, M. A. An argument against a role for Oct4 in somatic stem cells. *Cell Stem Cell* **1**, 359–360 (2007)
12. Hong, H. *et al.* Suppression of induced pluripotent stem cell generation by the p53-p21 pathway. *Nature* **460**, 1132–1135 (2009)
13. Hanna, J. *et al.* Direct reprogramming of terminally differentiated mature B lymphocytes to pluripotency. *Cell* **133**, 250–264 (2008)
14. Ohbo, K. *et al.* Identification and characterization of stem cells in prepubertal spermatogenesis in mice small star, filled. *Dev. Biol.* **258**, 209–225 (2003)
15. Holtfreter, J. Neural induction in explants which have passed through a sublethal cytolysis. *J. Exp. Zool.* **106**, 197–222 (1947)
16. Gerhart, J. Johannes Holtfreter's contributions to ongoing studies of the organizer. *Dev. Dyn.* **205**,

245–256 (1996)

17. Byrnes, W. M. Ernest Everett Just, Johannes Holtfreter, and the origin of certain concepts in embryo morphogenesis. *Mol. Reprod. Dev.* **76**, 912–921 (2009)

18. Gratama, J. W., Sutherland, D. R. & Keeney, M. Flow cytometric enumeration and immunophenotyping of hematopoietic stem and progenitor cells. *Semin. Hematol.* **38**, 139–147 (2001)

19. Inoue, K. *et al.* Inefficient reprogramming of the hematopoietic stem cell genome following nuclear transfer. *J. Cell Sci.* **119**, 1985–1991 (2006)

20. Ying, Q. L. *et al.* The ground state of embryonic stem cell self-renewal. *Nature* **453**, 519–523 (2008)

21. Tesar, P. J. *et al.* New cell lines from mouse epiblast share defining features with human embryonic stem cells. *Nature* **448**, 196–199 (2007)

22. Brons, I. G. *et al.* Derivation of pluripotent epiblast stem cells from mammalian embryos. *Nature* **448**, 191–195 (2007)

23. Kuroda, Y. *et al.* Isolation, culture and evaluation of multilineage-differentiating stress-enduring (Muse) cells. *Nature Protocols* **8**, 1391–1415 (2013)

24. Niwa, H. How is pluripotency determined and maintained? *Development* **134**, 635–646 (2007)

25. Watanabe, K. *et al.* Directed differentiation of telencephalic precursors from embryonic stem cells. *Nature Neurosci.* **8**, 288–296 (2005)

26. Kawasaki, H. *et al.* Induction of midbrain dopaminergic neurons from ES cells by stromal cell-derived inducing activity. *Neuron* **28**, 31–40 (2000)

27. Gouon-Evans, V. *et al.* BMP-4 is required for hepatic specification of mouse embryonic stem cell-derived definitive endoderm. *Nature Biotechnol.* **24**, 1402–1411 (2006)

28. Ohgushi, M. & Sasai, Y. Lonely death dance of human pluripotent stem cells: ROCKing between metastable cell states. *Trends Cell Biol.* **21**, 274–282 (2011)

29. Ohgushi, M. *et al.* Molecular pathway and cell state responsible for dissociation-induced apoptosis in human embryonic stem cells. *Cell Stem Cell* **7**, 225–239 (2010)

30. Murakami, K., Araki, K., Ohtsuka, S., Wakayama, T. & Niwa, H. Choice of random rather than imprinted X inactivation in female embryonic stem cell-derived extra-embryonic cells. *Development* **138**, 197–202 (2011)

31. Pera, M. F. & Tam, P. P. Extrinsic regulation of pluripotent stem cells. *Nature* **465**, 713–720 (2010)

32. Surani, M. A. & Barton, S. C. Development of gynogenetic eggs in the mouse: implications for parthenogenetic embryos. *Science* **222**, 1034–1036 (1983)

33. Wakayama, S. *et al.* Successful serial recloning in the mouse over multiple generations. *Cell Stem Cell* **12**, 293–297 (2013)

34. Nagy, A., Rossant, J., Nagy, R., Abramow-Newerly, W. & Roder, J. C. Derivation of completely cell culture-derived mice from early-passage embryonic stem cells. *Proc. Natl Acad. Sci. USA* **90**, 8424–8428 (1993)

35. Eakin, G. S., Hadjantonakis, A. K., Papaioannou, V. E. & Behringer, R. R. Developmental potential and behavior of tetraploid cells in the mouse embryo. *Dev. Biol.* **288**, 150–159 (2005)

36. Ogawa, K., Matsui, H., Ohtsuka, S. & Niwa, H. A novel mechanism for regulating clonal propagation of mouse ES cells. *Genes Cells* **9**, 471–477 (2004)

37. Hurtado, C. & De Robertis, E. M. Neural induction in the absence of organizer in salamander is mediated by MAPK. *Dev. Biol.* **307**, 282–289 (2007)

38. Hou, P. *et al.* Pluripotent stem cells induced from mouse somatic cells by small-molecule compounds. *Science* **341**, 651–654 (2013)

39. Eiraku, M. *et al.* Self-organizing optic-cup morphogenesis in three-dimensional culture. *Nature* **472**, 51–56 (2011)

40. Eilken, M. H., Nishikawa, S. & Schroeder, T. Continuous single-cell imaging of blood generation from haemogenic endothelium. *Nature* **457**, 896–900 (2009)

41. Jentsch, I., Geigl, J., Klein, C. A. & Speicher, M. R. Seven-fluorochrome mouse M-FISH for high-resolution analysis of interchromosomal rearrangements. *Cytogenet. Genome Res.* **103**, 84–88 (2003)

Download references

Acknowledgements

We thank S. Nishikawa for discussion and J. D. Ross, N. Takata, M. Eiraku, M. Ohgushi, S. Itoh, S. Yonemura, S. Ohtsuka and K. Kakiguchi for help with experiments and analyses. We thank A. Penvose and K. Westerman for comments on the manuscript. H.O. is grateful to T. Okano, S. Tsuneda and K. Kuroda for support and encouragement. Financial support for this research was provided by Intramural RIKEN Research Budget (H.O., T.W. and Y.S.), a Scientific Research in Priority Areas (20062015) to T.W., the Network Project for Realization of Regenerative Medicine to Y.S., and Department of Anesthesiology, Perioperative and Pain Medicine at Brigham and Women's Hospital to C.A.V.

Author information

Affiliations

Laboratory for Tissue Engineering and Regenerative Medicine, Brigham and Women's Hospital, Harvard Medical School, Boston, Massachusetts 02115, USA

Haruko Obokata, Koji Kojima, Martin P. Vacanti & Charles A. Vacanti

Laboratory for Cellular Reprogramming, RIKEN Center for Developmental biology, Kobe 650-0047, Japan

Haruko Obokata

Laboratory for Genomic Reprogramming, RIKEN Center for Developmental biology, Kobe 650-0047, Japan
Haruko Obokata & Teruhiko Wakayama

Laboratory for Organogenesis and Neurogenesis, RIKEN Center for Developmental biology, Kobe 650-0047, Japan
Yoshiki Sasai

Department of Pathology, Irwin Army Community Hospital, Fort Riley, Kansas 66442, USA
Martin P. Vacanti

Laboratory for Pluripotent Stem Cell Studies, RIKEN Center for Developmental biology, Kobe 650-0047, Japan
Hitoshi Niwa

Institute of Advanced Biomedical Engineering and Science, Tokyo Women's Medical University, Tokyo 162-8666, Japan
Masayuki Yamato

Present address: Faculty of Life and Environmental Sciences, University of Yamanashi, Yamanashi 400-8510, Japan.
Teruhiko Wakayama

Contributions
H.O. and Y.S. wrote the manuscript. H.O., T.W. and Y.S. performed experiments, and K.K. assisted with H.O.'s transplantation experiments. H.O., T.W., Y.S., H.N. and C.A.V. designed the project. M.P.V. and M.Y. helped with the design and evaluation of the project.

Competing financial interests
The authors declare no competing financial interests.

Corresponding authors
Correspondence to: Haruko Obokata or Charles A. Vacanti

Extended data figures and tables

Extended Data Figures

1. Extended Data Figure 1: Conversion of haematopoietic cells into *Oct4*-GFP$^+$ cells by a low-pH exposure. (292 KB)
   a, Optimization of pH conditions for *Oct4*-GFP induction. Five days after CD45-positive cells were exposed to acidic solution treatment at different pH, *Oct4*-GFP expression was analysed by FACS (n = 3, average±s.d.). **b**, Gating strategy for *Oct4*-GFP$^+$ cell sorting. Top: representative results 7 days after the stress treatment. Bottom: non-treated control. P3 populations were sorted and counted as *Oct4*-GFP$^+$ cells for all experiments. **c**, Controls for

FACS analysis. In *Oct4*-GFP$^+$ cell analysis, the grey and white histograms indicate the negative control (non-stress-treated *Oct4-gfp* haematopoietic cells) and the positive control (*Oct4-gfp* ES cells), respectively. Also, the green histograms indicate non-treated cells (left) and stress-treated cells at day 7 (right). In CD45$^+$ cell analysis, the grey and white histograms indicate the negative (isotype) and positive controls, respectively. The red histograms indicate non-stress-treated cells (left) and stress-treated cells at day 7 (right). **d**, *Oct4*-GFP$^+$ cell generation from various subpopulations of CD45$^+$ cells. Seven days after the stress treatment, *Oct4*-GFP expression was analysed by FACS ($n = 3$, average ± s.d.). Among total CD45$^+$ fraction and its subfractions of CD19$^+$, CD90$^+$, CD34$^+$ and CD34$^-$ cells, the efficacy of CD34$^+$ cells was significantly lower than the others. $P < 0.05$ by the Newman–Keuls test and $P < 0.01$ by one-way ANOVA. **e**, Comparison of culture conditions for low-pH-induced conversion. Stress-treated cells were cultured in various media. The number of *Oct4*-GFP-expressing clusters was counted at day 14 ($n = 3$, average ± s.d.). ***$P < 0.001$ (B27+LIF versus all other groups); Tukey's test. In the case of 3i medium, although the clusters appeared at a moderate efficiency, they appeared late and grew slowly. ACTH, ACTH-containing ES medium; ES+LIF+FBS, 20% FBS+LIF-containing ES culture medium; B27, DMEM/F12 medium containing 2% B27; B27+LIF, DMEM/F12 medium containing 2% B27+LIF; EpiSC, EpiSC culture medium containing Fgf2+activin. **f**, Signalling factor dependency of STAP cell generation. Growth factors that are conventionally used for pluripotent cell culture such as LIF, activin, Bmp4 and Fgf2 were added to basal culture medium (B27-supplemented DMEM/F12) in different culture phases (days 0–7, 2–7 and 4–7), and *Oct4*-GFP expression was analysed by FACS at day 7 ($n = 3$, average ± s.d.). **g**, **h**, Time course of apoptosis after the low-pH exposure. Stress-treated cells and non-stress-treated control cells were stained with CD45, annexin-V and propidium iodide at day 0 (immediately after stress treatment), day 3 and day 7. **g**, Blue bars, GFP$^+$CD45$^-$; orange bars, GFP$^-$CD45$^+$. Percentages in total cells included propidium-iodide-positive cells. **h**, Annexin-V-positive cells in these cell populations were analysed by FACS.

2. Extended Data Figure 2: Phenotypic change during STAP cell conversion. (231 KB)
a, Oct4 protein expression in STAP cells was detected by immunostaining at day 2 (left) and day 7 (right). **b**, Live cell imaging of STAP conversion (grey, CD45 antibody; green, *Oct4*-GFP). See Methods for experimental details to monitor live CD45 immunostaining. **c**, Immunostaining of a parental CD45$^+$ cell (left) and an *Oct4*-GFP$^+$ cell (right). Scale bar, 10 μm. **d**, EdU uptake assay ($n = 3$, average ± s.d.). **e**, Schematic of *Tcrb* gene rearrangement. **f**, T-cell-derived STAP cells. Scale bar, 100 μm. **g**, Genomic PCR analysis of (D)J recombination at the *Tcrb* gene of T-cell-derived STAP cells. G.L. is the size of the non-rearranged germline type, whereas the smaller ladders correspond to the alternative rearrangements of J exons (confirmed by sequencing). Negative controls (ES cells), positive controls (lymphocytes) and T-cell-derived STAP (two independent preparations on d7) are indicated.

3. Extended Data Figure 3: Gene expression analyses during STAP conversion and endoderm differentiation assay. (213 KB)

a, Expression of pluripotency marker genes in STAP cells derived from T cells (*n* = 3, average ±s.d.). **b**, Expression of pluripotency marker genes in STAP cells. In this experiment, *Oct4*-GFP$^+$ cells seen in live cell imaging (Extended Data Fig. 2b) were analysed to confirm their conversion into STAP cells (*n* = 3, average±s.d.). **c**, Haematopoietic marker expression during STAP conversion from CD45$^+$ cells (*n* = 3, average±s.d.). **d**, Formation of visceral endoderm-like surface epithelium in differentiating STAP cluster on day 2 (left) and day 8 (right). Scale bars, 50μm.

4. Extended Data Figure 4: Teratoma formation assay and characterization of *Oct4*-GFP-dim cells. (265 KB)
a–**c**, Teratomas formed from STAP cell clusters included neuroepithelium (**a**), striated muscle (**b**) and pancreas (**c**; right, high-magnification view showing a typical acinar morphology and ductal structures). Scale bars, 100μm. **d**, Teratoma-forming ability of *Oct4*-GFP$^+$ and *Oct4*-GFP-dim cells (isolated by FACS, top). *Oct4*-GFP$^+$ cells, but not *Oct4*-GFP-dim cells, efficiently formed teratomas (table at the bottom). However, because STAP cells were dissociation-intolerant, the teratoma-forming efficiency of dissociated *Oct4*-GFP$^+$ cells was lower than that of non-dissociated STAP cell clusters. **e**, Gene expression of *Oct4*-GFP$^+$ and *Oct4*-GFP-dim cells (*n* = 3, the average±s.d.). Haematopoietic marker gene expression (left) and early lineage marker gene expression (right) are shown.

5. Extended Data Figure 5: *In vitro* characterization of STAP cells. (430 KB)
a, Immunostaining for Ki67 and BrdU. STAP cell clusters (top) and ES cell colonies (bottom) are shown. For BrdU uptake, BrdU was added into each culture medium (10μM) for 12h until fixation. Scale bar, 100μm. **b**, Transformation assay by soft agar culture. Neither *Oct4*-GFP$^+$ nor *Oct4*-GFP-dim cells showed colony formation in soft agar, whereas ES cells and STAP stem cells showed anchorage-independent growth in the same LIF-B27 medium. Scale bar, 100μm. Proliferated cells were lysed and the amount of DNA in each well was estimated by chemical luminescence (graph). *n* = 3 , average±s.d. **c**, No substantial change in chromosome number was seen with STAP cells in the CGH array. Genomic DNA derived from CD45$^+$ cells (male) was used as reference DNA. The spikes (for example, those seen in the X chromosome) were nonspecific and also found in the data of these parental CD45$^+$ cells when the manufacturer's control DNA was used as a reference. **d**, qPCR analysis for pluripotency markers that highly express in ES cells, but not in EpiSCs. Average±s.d. **e**, Immunostaining of markers for mouse EpiSC and ES cells. Scale bar, 100 μm. **f**, **g**, H3K27me3$^+$ foci in female cells, which are indicative of X-chromosomal inactivation. These foci were not observed in male cells. Scale bar, 10μm. In the case of female STAP cells, ~40% of cells retained H3K27me3$^+$ foci (**g**). ***P*<0.001; Tukey's test. *n* = 3, average±s.d. Although nuclear staining looked to be higher in STAP cells with H3K27me3$^+$ foci (**f**), this appeared to be caused by some optical artefacts scattering from the strong focal signal. **h**, qPCR analysis for the tight junction markers *Zo-1* and claudin 7, which were highly expressed in EpiSCs, but not in ES cells or STAP cells. ***P*<0.01; ns, not significant; Tukey's test; *n* = 3, average±s.d.

6. Extended Data Figure 6: Conversion of somatic tissue cells into STAP cells. (371 KB)
a, Alkaline phosphatase expression of STAP cells derived from adipose-derived mesenchymal cells. Scale bar, 100 μm. **b**, E-cadherin expression of STAP cells derived from adipose-derived mesenchymal cells. Scale bar, 50 μm. **c**, FACS sorting of dissociated neonatal cardiac muscle cells by removing $CD45^+$ cells. **d**, Cardiomyocyte marker gene expression during STAP conversion from cardiomyocytes (n = 3, average ± s.d.).

7. Extended Data Figure 7: Generation chimaeras with STAP cells. (170 KB)
a, 2N chimaeras generated with STAP cells derived from *Oct4-gfp* C57BL/6 mice (left) and 129/Sv × C57BL/6 F_1 mice (right). **b**, Generation of chimaeric mice from STAP cells by cluster injection. STAP cells used in the experiments above were generated from $CD45^+$ lymphocytes of multiple neonatal spleens (male and female tissues were mixed). *All fetuses were collected at 13.5 d.p.c. to 15.5 d.p.c. and the contribution rate of STAP cells into each organ was examined by FACS. **The contribution of STAP cells into each chimaera was scored as high (>50% of the coat colour of GFP expression). ***B6GFP: C57BL/6 mouse carrying *cag-gfp.* **c**, Production of offspring from STAP cells via germline transmission. Chimaeras generated with 129/Sv × B6GFP STAP cells (obtained from the experiments shown in **b**) were used for germline transmission study. **d**, 4N embryos at E9.5 generated with STAP cells derived from F_1 GFP mice (B6GFP and DBA/2 or 129/Sv). B6GFP, C57BL/6 mouse carrying *cag-gfp*.

8. Extended Data Figure 8: Molecular and cellular characterization of STAP stem cells. (347 KB)
a, Compatibility of 2i conditions with STAP stem-cell derivation from STAP cells and STAP stem-cell maintenance. STAP stem cells could not be established directly from STAP cells in 2i + LIF medium (top). However, once established in ACTH medium, STAP stem cells were able to survive and expand in 2i + LIF medium. Scale bar, 100 μm. **b**, Q-band analysis (n = 4; all cell lines showed the normal karyotype). **c**, Multicolour FISH analysis (n = 8; all cell lines showed the normal karyotype) of STAP stem cells. **d**, Methylation status of the *Oct4* and *Nanog* promoters. **e**, Electron microscope analysis of STAP stem cells. Scale bar, 1 μm. **f**, **g**, Beating cardiac muscle (mesoderm; 38%, n = 8). Red line indicates an analysed region for kymograph (**g**). **h**, Clonability of STAP stem cells. Clonal expansion from single STAP stem cells was performed. Pluripotency of clonal cell lines was confirmed by teratoma formation assay, showing the formation of neuroectoderm (left), muscle tissue (middle) and bronchial-like epithelium (right). Scale bar, 100 μm. **i**, Production of chimaeric mice from STAP stem-cell lines using diploid embryos. *These STAP stem-cell lines were generated from independent STAP cell clusters. **j**, Production of mouse chimaeras from STAP stem-cell lines by the tetraploid complementation method. *These STAP stem-cell lines were generated from independent STAP cell clusters. **k**, No H3K27me3-dense foci are seen in female STAP stem cells (n = 50; the $CD45^+$ cell is a positive control). Scale bar, 10 μm.

9. Extended Data Figure 9: Effects of various stressors on STAP conversion. (123 KB)
a, Percentages of *Oct4*-GFP-expressing cells 7 days after stress treatment. Somatic cells were isolated from various tissues and exposed to different stressors. *Oct4*-GFP expression was

analysed by FACS. **b**, Oct4 and *Oct4*-GFP expression induced in the reflux oesophagitis mouse model as an *in vivo* acid exposure model (top, experimental procedure). Oct4, but not Nanog, expression was observed in the oesophageal epithelium exposed to gastric acid (75% of 12 operated mice).

Supplementary information

Video

1. Video 1: Live imaging of low-pH-treated $CD45^{+}$cells (22.67 MB, Download)
   DIC images during day 0 – day 7, overlaid with *oct3/4::*GFP (green). A strong contrast of DIC (as compared to video 2) was applied to imaging so that lamellipodia-like processes (frequently seen on and after day 4) could be viewed easily.

2. Video 2: Live imaging of low-pH-treated $CD45^{+}$cells (another view) (11.62 MB, Download)
   DIC images during day 0 – day 6, overlaid with *oct3/4::*GFP (green). The interval of imaging was half (15 min) of that of video 1 (the overall speed of the video is three-times slower than video 1). In this view field where the cell density was relatively low, behaviours of individual cells were more easily seen. In this case, forming clusters were slightly smaller in size.

3. Video 3: STAP cell-derived embryo (E10.5) from 4N blastocyst injection (1.61 MB, Download)
   STAP cells with constitutive GFP expression were injected into 4N blastocysts and produced normal embryos with heart beating.

4. Video 4: Beating cardiac muscle generated from STAP-SCs *in vitro* Bright-field image. (2.42 MB, Download)

PDF files

1. Supplementary Information (102 KB)
   This file contains Supplementary Table 1.

Comments

2014-01-29 07:00 AM

Donald Newgreen said: There is a recognised phenomenon of a variety of cellular stresses inducing changes like epithelial-mesenchymal transition (EMT) in cancerous, precancerous and normal cells. It is presumed to be in part an adaptive protective response; EMT often confers resistence to various cell death stimuli. The EMT has been related to induced expression of stem cell characteristics (Mani, et al. Cell 133, 704-715). This may have snapped into this program. Nevertheless the precautionary TGTBT principle applies for the present (ie. too good to be true). There's always cold fusion to remember.

Subscribe to comments

Nature ISSN 0028-0836 EISSN 1476-4687